

# CONCEPTUAL DESIGN OF TRITIUM REMOVAL FACILITY FOR FHRS

**Xiao Wu, David Arcilesi, Xiaodong Sun, Richard Christensen**

Nuclear Engineering Program

Ohio State University

Columbus, OH 43210, USA

wu.1925@osu.edu, arcilesi.1@osu.edu, sun.200@osu.edu, christensen.3@osu.edu

**Piyush Sabharwall**

Idaho National Laboratory

Idaho Falls, ID 83415, USA

piyush.sabharwall@inl.gov

## ABSTRACT

Tritium control is one of the most significant issues in Fluoride-salt-cooled High-temperature Reactors (FHRs). Due to primarily neutron activation of the primary coolant FLiBe, a considerable amount of tritium is generated in the primary loop. Tritium has excellent transport properties that allow it to move into the environment, which would lead to health concerns to human beings and other living creatures. Thus it is necessary to control and manage the generated tritium. In this paper, several design concepts for a primary tritium removal facility are described and evaluated. The facility is designed for primary loop and outside reactor core. The designs include a gas bubble purging system, a packed bed absorbing system, and a heat exchanger geometry. Computer simulation was performed to determine the dimensions of the facility. In this study, the AHTR pre-conceptual design by the Oak Ridge National Laboratory was adopted as the FHR reference design. Primary comparisons of different designs were based on the computer simulation results. Those concepts giving the best performance will be chosen for further design refinement and evaluation, taking the entire primary loop into account.

## KEYWORDS

FHRs; Tritium removal; Facility design; Separation

## 1. INTRODUCTION

The Fluoride salt-cooled High-temperature Reactor (FHR) is an advanced reactor concept that combines advantageous technologies from several Generation-IV reactors. In the FHR, the liquid salt of Molten Salt Reactors (MSRs), the graphite-matrix coated-particle fuel of High-Temperature Gas-cooled Reactors (HTGRs), and the pool type design and passive safety system of Sodium Fast Reactors (SFRs) are incorporated. Due to primarily the neutron activation of the primary coolant FLiBe, a considerable amount of tritium is expected to be produced in FHRs. The amount of tritium production has been estimated to be 5,000 Ci/day at startup in an FHR with a power rating of 2,400 MWth, while the number in a typical 1000 MWe commercial PWR is 1.9 Ci/day [1]. Permeation of tritium is a critical issue in FHR operation. If tritium is left to accumulate in the primary loop, it will diffuse through the loop pipe walls and the intermediate heat exchangers, and be released into the environment. Therefore, tritium removal from the

primary loop and proper tritium control are important issues to be solved. To accommodate various types of reactor cores, a tritium control system on the primary loop, but outside the core is preferred.

Tritium extraction from the primary fluoride salt (FLiBe) of an FHR is fundamentally a chemical separation process. Consequently, transport theory of chemical species has been applied to this problem. Diffusion of a dilute chemical species is a mass transport process which is very similar to a heat transfer processes. In a mass transfer processes, it is the chemical potential that provides the driving force, functioning as the counterpart of temperature in heat transfer problems. Corresponding parameters of mass and heat transfer are listed in Table I [2].

**Table I. Mass and Heat Transfer Parameters**

No.	Mass transfer	Heat transfer
1	Reynolds number $Re = \frac{\rho v D}{\mu}$	Reynolds number $Re = \frac{\rho v D}{\mu}$
2	Schmidt number $Sc = \frac{\mu}{\rho D_{AB}}$	Prandtl number $Pr = \frac{c_p \mu}{k} = \frac{\nu}{\alpha}$
3	Sherwood number $Sh = \frac{k_s D}{D_{AB}}$ etc.	Nusselt number $Nu = \frac{h D}{k}$
4	Peclet number $Pe = Re Sc$	Peclet number $Pe = Re Sc$
5	Grashot number $Gr = g L^3 \left(\frac{\rho}{\mu}\right)^2 \left(\frac{\Delta \rho}{\rho}\right)$	Grashot number $Gr = g D^3 \left(\frac{\rho^2}{\mu^2}\right) \beta (\Delta T)$ $\beta = \text{coefficient of expansion}$
6	Stanton number $St = \frac{Sh}{Re Sc} = \frac{Sh}{Pe}$	Stanton number $St = \frac{Nu}{Re Pr} = \frac{Sh}{Pe}$

In chemical engineering, common separation methods can be divided into the following categories according to the contact phases: 1) gas-liquid separation; 2) solid-liquid separation; 3) liquid-liquid separation. In the current problem, the first two methods are generally simpler in operation than the third one. Thus the gas-liquid separation process and the solid-liquid separation process were investigated in this study in more detail.

An investigation into chemical separation process and heat exchangers, resulted in several designs of a tritium removal facility being proposed. The key rules to follow in the designing process are:

1. To maximize the contacting surface area of the molten fluoride salt and extracting material, i.e., the surface area of stainless steel in most designs or gas bubbles in a helium purging extraction design.

- To increase the turbulence of the molten fluoride salt flow. Thus the gradient of  $T_2$  concentration from the channel center to the diffusion boundary can be flattened, decreasing the diffusion resistance of  $T_2$  in the molten salt.

## 2. DESIGN AND COMPUTER SIMULATIONS OF TRITIUM REMOVAL FACILITIES

### 2.1. Helium Gas Purging Method

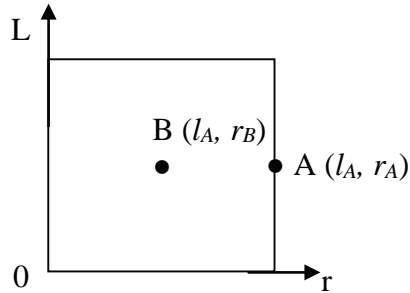


Figure 1. Implicit 2-D model

In this design, helium gas bubbles are injected into the molten salt as bubbles from the bottom, and the bubbles rise upward due to buoyancy and inertia, extracting  $T_2$  molecules, which are dissolved in the molten salt. The molten salt can be stagnant, flowing upward, or flowing downward. However, to maximize the extraction efficiency, it is recommended that the salt and gas bubbles move in a counter-current manner. In this way, similar to a counter-current flow heat exchangers, the tritium concentration difference between the molten salt and gas can be maximized.

Helium was selected as the purging gas mainly because of its chemical stability under high temperatures, as well as its accessibility. In order to minimize heat loss to the purging gas, helium would be heated up to the molten salt core outlet temperature before being injected into the system.

A two-dimensional (2-D) implicit model was built to evaluate the efficiency of this design and determine the required bubble dimensions and concentrations. This model is modified from the model “Packed Bed Reactor” in the COMSOL model library [3]. FLiNaK was used for the molten salt and helium for the purging gas (namely, the rising bubbles) in the simulation. For the diffusing gas,  $H_2$  was used instead of  $T_2$  because of limited data of  $T_2$  transport behavior.

The facility was modeled as a simple square, as shown in Figure 1, with the  $L$  axis representing the height of the facility, and the  $r$  axis the radius dimension of a single helium bubble. In this model, all the bubbles were assumed to have the same radius. For example,  $H_2$  concentration at point A is the average  $H_2$  concentration in FLiNaK in the flow direction at  $l_A$  from the inlet of the facility. Also, it is the  $H_2$  concentration at the surface of a single bubble at location  $l_A$ . While the  $H_2$  concentration at point B is the  $H_2$  concentration inside the bubble, and the distance from point B to the surface of the bubble is  $r_B$ . The reactor model and the bubble model are coupled through the flux of  $H_2$  being transported between molten fluoride salt and purging gas bubbles. This flux is modeled by a mass source in the bubble domain and a mass sink in the reactor domain. By equating the  $H_2$  flux leaving FLiNaK to that entering a single He bubble, and taking into account the diffusion of  $H_2$  in the bubble, the model ensures the mass balance of  $H_2$ .

Bubbly flow can only contain no more than 15-20% volume fraction of bubbles before the bubbles start to collide and coalesce, decreasing the mass transfer surface area. This highly constrains the total interface surface area between the molten salt and the gas bubbles. One way to compensate for this drawback is to use as small bubbles as possible. Thus in this simulation, the bubble diameter was set as 1 mm and the volume fraction was set as 10%. The flow rate of molten FLiNaK was set as 0.2 m/s. According to simulation results, such a bubbly flow purging system will need a 200-meter flow length to accomplish the required removal of tritium (99% tritium removal).

## 2.2. Stainless Steel Packed Bed Scrubber

One widely used method in chemical industry is the packed bed reactor. In a typical packed bed reactor, the vessel is filled with catalyst pellets, and the reaction takes place on the catalyst's surface. As it shows some similarities with tritium removal, the idea of packed bed reactors is evaluated. A vessel is filled with stainless steel balls which would absorb  $T_2$ . As the concentration of  $T_2$  inside a stainless steel ball increases, its ability to absorb  $T_2$  will decrease accordingly. When the  $T_2$  concentration in the stainless steel ball reaches a limiting concentration, it should be replaced by a new ball. For simplicity in this paper, this situation is referred to as the "saturation" of the stainless steel ball, though the  $T_2$  concentration in the stainless steel ball has not yet reached its solubility limit. The stainless steel balls can be stationary or circulating. These contaminated steel balls will be recycled and cleaned up after reaching saturation.

Compared with a bubble column, a packed bed uses metal balls, which avoids the bubble merging issue, thus maintaining a high mass transfer surface area. However, due to the requirement of maintaining a high surface area to volume ratio, a large number of metal balls are needed in a packed bed scrubber.

Graphite spheres are also investigated as a tritium absorber. However, since graphite has a  $T_2$  diffusivity nearly five times smaller than stainless steel, it theoretically requires a longer time to take up  $T_2$  from the molten salt. It means that under the same molten salt flow rate, a column filled with graphite balls needs longer flow distance than one with stainless steel balls to achieve the same level of  $T_2$  removal. In this sense, graphite is less effective than stainless steel for this application. Also, the moderating effect of graphite on the neutron flux would need to be carefully evaluated.

For the computer simulations, the model used was that shown in Figure 1. The properties of helium were replaced by those of stainless steel. Hydrogen again replaced tritium in these simulations. Since,  $H_2$  diffusion in stainless steel is much slower than that in helium, a decrease in efficiency was expected.

Figure 2 and Figure 3 present the concentration distribution of  $H_2$  in the molten salt at different times for two different models. The  $x$  axis is the length of the pipe in the direction of molten salt flow. As expected, the  $H_2$  concentration in the molten salt starts at an initial level at the inlet ( $x=0$ ), and decreases as it flows through the packed bed. Also, the  $H_2$  concentration at the same location increases as time passes. Meanwhile, the  $H_2$  concentration in the steel balls constantly increases. The objective of the facility is to achieve at least 99% tritium removal, which corresponds to  $1.8 \times 10^{-9}$  mol/m<sup>3</sup> when the hydrogen production rate is  $1.8 \times 10^{-7}$  mol/m<sup>3</sup>-s [4]. Thus, once the hydrogen concentration at the outlet cannot be reduced to the level of  $1.8 \times 10^{-9}$  mol/m<sup>3</sup>, the packed bed is "saturated" and has to be replenished. As shown in Figure 2, which lists facility dimensions and operation conditions, it would take 50 s for the packed bed to saturate. Similarly in Figure 3, it would take 150 s for that facility to saturate.

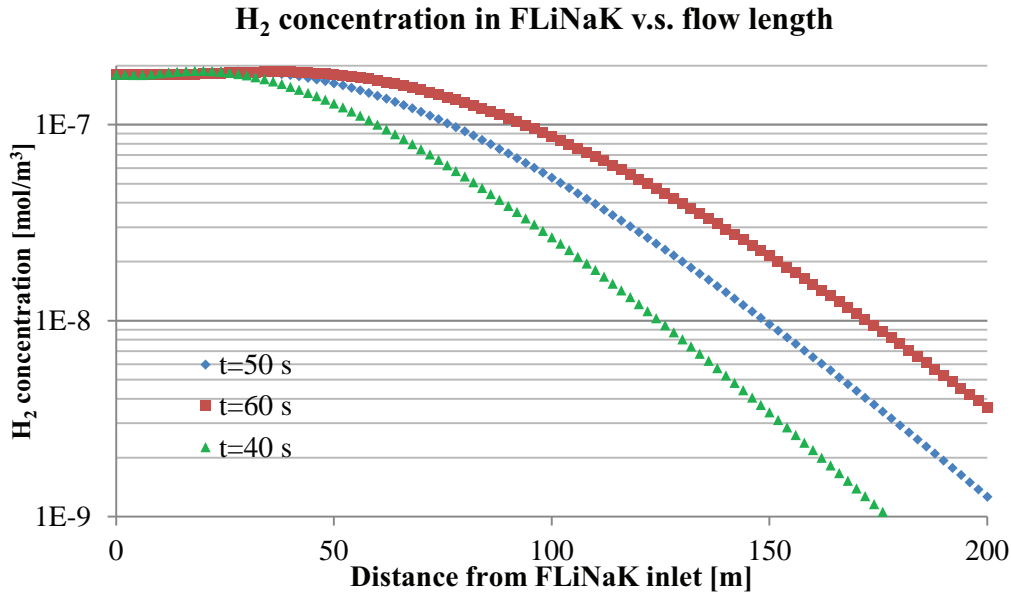


Figure 2. H<sub>2</sub> concentration distribution of model D20S40c (see Table II)

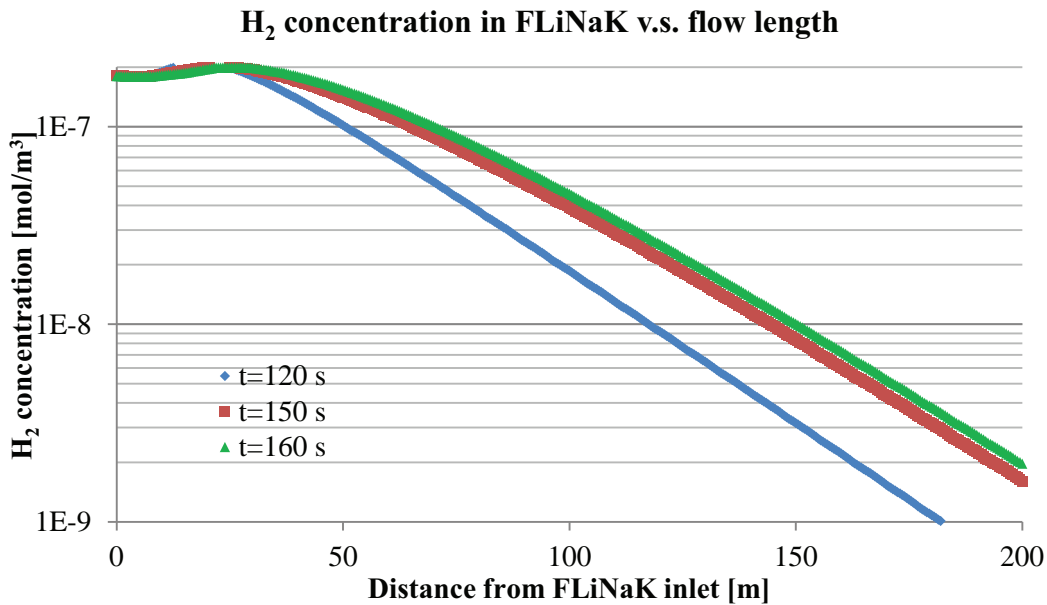


Figure 3. H<sub>2</sub> concentration distribution of model D36S40b (see Table II)

In order to make the facility design feasible, a long saturation time is ideal with practical dimensions and operation conditions. Several models have been applied in the simulations and the summary of the simulation results are shown in Table II. The AHTR pre-conceptual design [4] is used for evaluation of the tritium removal efficiency of the models. In the simulations, two sets of commercial pipe sizes (outer diameter 20 in, Schedule 40 and outer diameter 36 in, Schedule 40) were used.  $A_{ratio}$  is the ratio of pipe

inner diameter to the stainless steel ball diameter, which is called the aspect ratio.  $\epsilon$  is the porosity, defined as the fraction of the volume that is not taken by the stainless steel balls. The stainless steel balls were assumed to have a slightly looser packing pattern with a porosity of 40% compared to the densest packing. Thus the only dimension unfixed is the total length of pipe needed. The length of the proposed facility needed to decontaminate the molten salt flow rate proposed by the AHTR pre-conceptual design [4], is listed in the right most column of Table II.

**Table II. Sample packed bed scrubber dimensions and operation conditions**

Model	$A_{ratio}$	$\epsilon$	Pipe Outside Diameter [in]	Schedule	Pipe Inner Diameter [in]/[m]	Radius of metal balls [in]/[m]	Salt flow rate Q [m <sup>3</sup> /s]	Salt flow velocity U [m/s]	Re (for FLiNaK/FLiBe) [10 <sup>4</sup> ]	Q by AHTR Design [m <sup>3</sup> /s]	Total Length of Pipe Needed [m]
D20S40a	50	0.4	20	40	18.814/0.4779	0.309/0.075	0.5	6.975	7/3.625	5.54	2200
D20S40b	50	0.4	20	40	18.814/0.4779	0.309/0.0075	0.125	1.7425	1.75/1.53		8800
D20S40c	79.65	0.4	20	40	18.814/0.4779	0.0984/0.0025	0.125	1.7425	0.6/0.302		8800
D36S40a	50	0.4	36	40	34.5/0.8763	1.74/0.0442	0.125	0.5175	1.0513/0.5229		8800
D36S40b	79.65	0.4	36	40	34.5/0.8763	0.0984/0.0025	0.125	0.5175	0.0803/0.0985		8800

From the different models in Table II, it can be seen that for a cylindrical packed bed with a 36 in (0.91 m) outer diameter with a radius of 0.0098 in (2.5 mm) and 200 m length, it takes about 3 minutes for stainless steel balls to reach saturation. There are two ways to increase the time before the stainless steel balls saturate. The first is to increase the facility's cross section area. Since the volumetric flow rate of the molten salt is set constant, the flow velocity will decrease accordingly. Thus it will take the stainless steel balls longer to become saturated. The second way is to increase the pipe length. With this approach, the pipes can be bent or curved to reduce the dimension of the facility. This model again shows that obtaining a large mass transfer surface area to volume ratio is a key issue for the tritium removal facility design.

### 2.3. Finned Plate Tritium Removal Facility Design

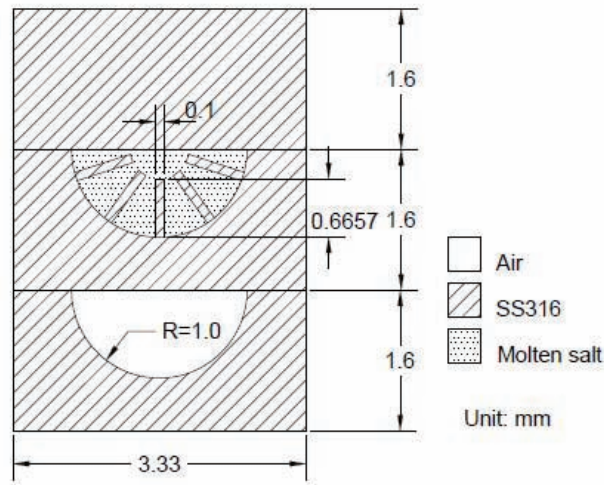


**Figure 4. Cross-sectional view of finned plate tritium removal facility model (unit cell)**

In this method, the geometry resembles a plate type compact heat exchanger. By adding fins in the molten salt flow channel, the surface area per unit volume on the salt side was significantly increased. The cross-sectional view of the two flow passages is shown in Figure 4.

Stainless steel 316 was used as the plate material. Molten salt flows in the finned semi-circular channels, and the other channels contain the purging gas. The dimensions used in this simulation ensured a large surface area to volume ratio. Thus the dimensions used in the current simulation are not practical or manufacturable. The diameters of the both types of flow channels are 2 mm, and the pitch of the channels on the same plate is 3 mm. The plate thickness is set to be 0.8 times of the channel diameter [5], namely, 1.6 mm as shown in Figure 4. For modeling simplicity, the fins in the molten salt channels are assumed to be straight fins, and also made of stainless steel 316. Five fins are distributed radially and uniformly in each salt channel, with 0.66 mm in height and 0.1 mm in thickness. The total length of the flow path is 200 m. In this design, the mass transfer area per unit volume on the molten salt side reaches 738 m<sup>2</sup>/m<sup>3</sup>.

For the computer simulation, FLiNaK and air were used as the fluids for the molten salt and the purging gas, respectively. Hydrogen was used instead of Tritium. Similar to the previous designs, the helium or air would be heated before entering into the facility. Air could be a candidate for the purging gas as long as the hydrogen concentration at the outlet of the facility did not reach the explosion limit and the oxygen did not cause corrosion concerns. The mean velocity of the molten salt in the channels is 0.1 m/s, while that of the purging gas is 0.5 m/s. Both flows are in the laminar flow regime.

The simulation results shows that this design fails to achieve satisfactory tritium removal efficiency. However, in Figure 5, cut views at different positions of H<sub>2</sub> concentration show the diffusion process. The numbers below each cross-sectional view represent the non-dimensional flow length.

$$x = \frac{\text{Distance from the salt inlet}}{\text{Total flow length}} \quad (2)$$

As can be seen from the figures, the concentration gradient was mainly in the molten salt domain. As FLiNaK flows forward, H<sub>2</sub> close to the stainless steel surfaces diffuses out of FLiNaK quickly, while the H<sub>2</sub> concentration in the bulk stays at a relatively high level. Since the flow is laminar, not much mixing happens in the flow. Thus the slow permeation of hydrogen in the molten salt prohibits the H<sub>2</sub> from being extracted.

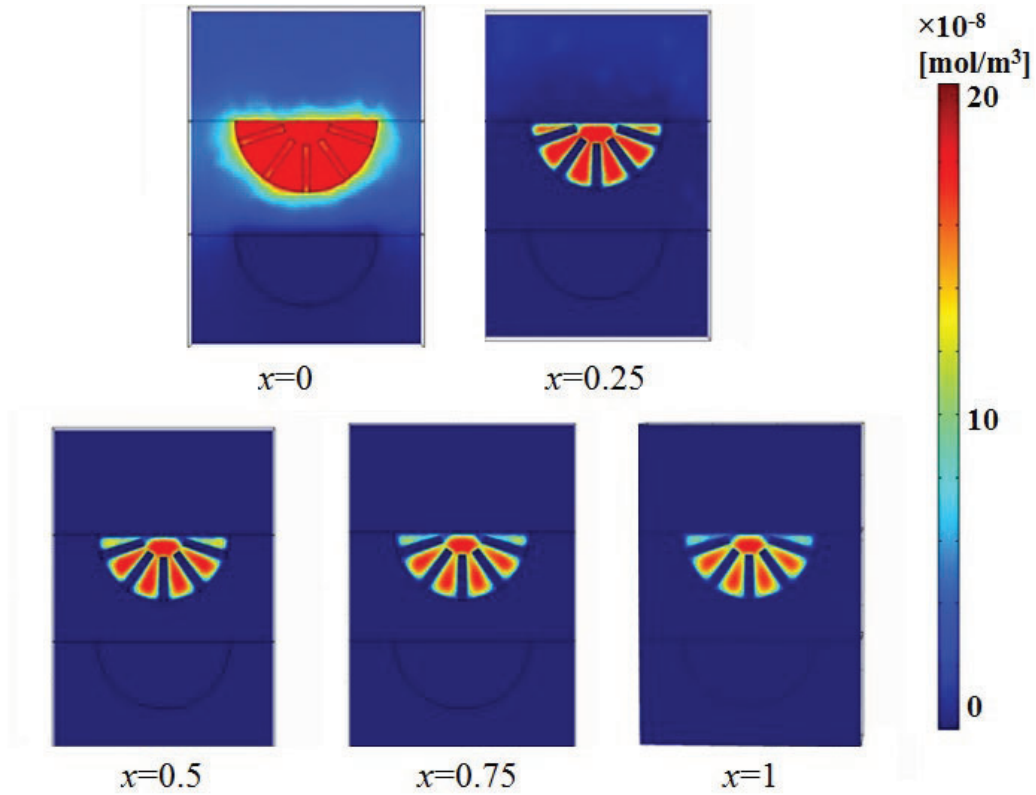
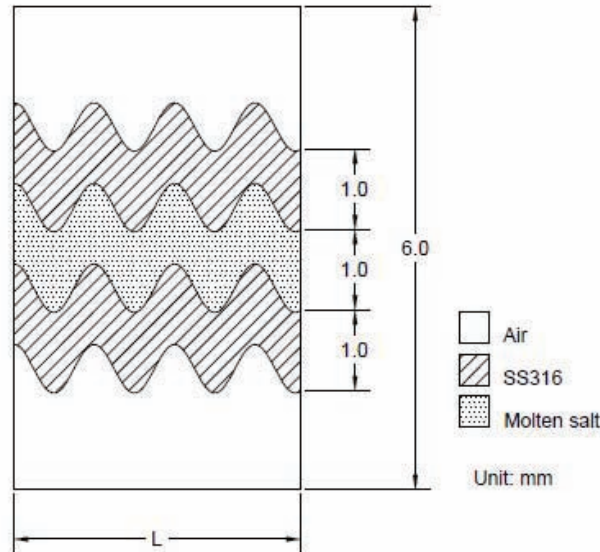


Figure 5. Cross-sectional views of the H<sub>2</sub> concentration distribution in the flow direction

#### 2.4. Wavy-channel Plate Design

Similar to the finned plate design, a wavy-channel plate design was also examined based on a plate-type compact heat exchange. Figure 6 shows the cross-sectional view of the design. There are five layers in total in Figure 6, from the top to bottom, the second and fourth layers are the base structural plates made of stainless steel 316. On the top and bottom of the two plates are the path ways for the purging gas, while the molten salt flows between the plates.



**Figure 6. Cross-sectional view of 2-D wavy-channel plate design (Unit cell)**

The thickness of the stainless steel plates is 1.0 mm, as well as the height of molten salt flow path. For simulation simplicity, the curvature of the plates is expressed by a sine function

$$y = 0.3 \times \sin\left(\pi x^2 + \frac{\pi}{2}\right) \quad (1)$$

where  $x$  is the distance from the inlet of the molten salt.

FLiNaK and air were used as the fluids for the molten salt and the purging gas, respectively. The molten salt flow rate was 0.1 m/s, and the air flow velocity in the channel was 0.5 m/s in the same direction as the molten salt. Hydrogen was used in the simulation instead of Tritium. Both fluids are in the laminar flow regime. As to the  $H_2$  diffusion conditions, no flux boundary condition was assigned to the top and bottom boundaries, and the stiff-spring boundary condition is assigned at the interfaces of adjacent diffusion domains.

Considering the efficiency of computer simulation, the length (in the  $x$  direction) of the model was set to be 100 mm. The inlet  $H_2$  concentration was set at the same level with the average  $H_2$  production rate suggested by the AHTR pre-conceptual design, which was  $1.8 \times 10^{-7}$  mol/m<sup>3</sup>-s [4]. After it reached a steady state, the outlet concentration at the center line of the molten salt flow was used as the inlet concentration for the next calculation. This process was repeated five times, as shown in Table III. In this way, the  $H_2$  diffusion behavior in a long channel can be approximately modeled using shortened geometry.

Figure 7 shows the distribution of  $H_2$  concentration in the model at the steady state. The red color represents a higher concentration of  $H_2$  and blue represents lower  $H_2$  concentrations. It can be explained in details as

1.  $H_2$  concentration distribution in the stainless steel plate is highest near the start of a valley nearest the molten salt region, but decreases quickly towards the air side.

2. Maximum H<sub>2</sub> concentration in the molten salt shows a wavy curve in accordance with the shape of the stainless steel plates.
3. In the stainless steel domain, near the surface which counters the molten salt flow, the H<sub>2</sub> concentration is clearly higher than that near the surface on the other side.

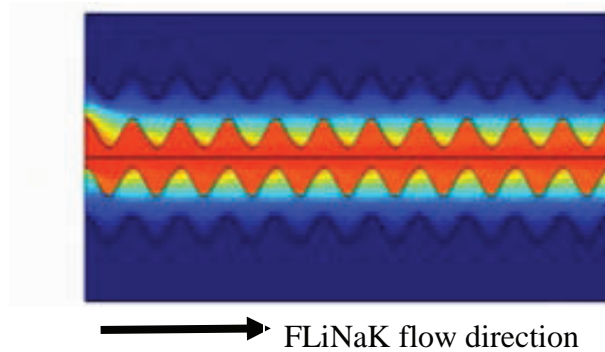


**Figure 7. H<sub>2</sub> concentration distribution**

Simulation results are listed in Table III. A 0.5% decrease in H<sub>2</sub> concentration in the molten FLiNaK is observed after the first 100-mm flow length. Also the difference between inlet and outlet H<sub>2</sub> concentration decreases as the flow length increases, as shown in Figure 8. The reason for the decrease in hydrogen removal is the decrease of mass transfer driving force as the molten salt flows forward. From Figure 8 the trend of H<sub>2</sub> concentration decrease with the total flowing length is almost a straight line. Thus the average amount of H<sub>2</sub> being removed would be  $4.5 \times 10^{-9}$  mol/m<sup>3</sup>. Accordingly, to reach the goal of 99% H<sub>2</sub> removal, the total length of flow needed is 39.6 m. Compared to previous design concepts that have been simulated, the wavy-channel plate design results in a relatively small facility size and is very promising.

**Table III. Results of the wavy plate model**

	Inlet concentration $\times 10^{-7}$ [mol/m <sup>3</sup> ]	Outlet concentration $\times 10^{-7}$ [mol/m <sup>3</sup> ]	$ \Delta $ $\times 10^{-7}$ [mol/m <sup>3</sup> ]
<b>1</b>	1.8	1.71	0.09
<b>2</b>	1.71	1.625	0.085
<b>3</b>	1.625	1.54	0.085
<b>4</b>	1.54	1.46	0.08
<b>5</b>	1.46	1.393	0.067
<b>6</b>	1.393	1.3285	0.0645
<b>7</b>	1.3285	1.2664	0.0621
<b>8</b>	1.2664	1.2066	0.0598
<b>9</b>	1.2066	1.1491	0.0575
...	...	...	...
<b>Last</b>		0.018 (99% removal)	

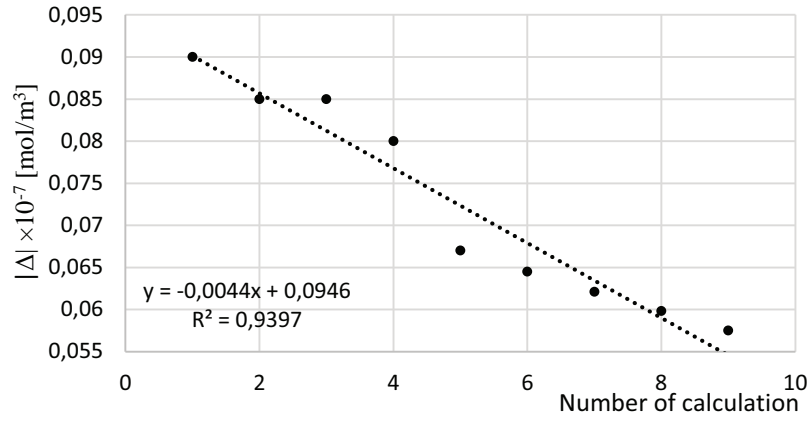


**Figure 8. H<sub>2</sub> concentration decrease in each calculation**

## 2.5. Cross-Flow Design

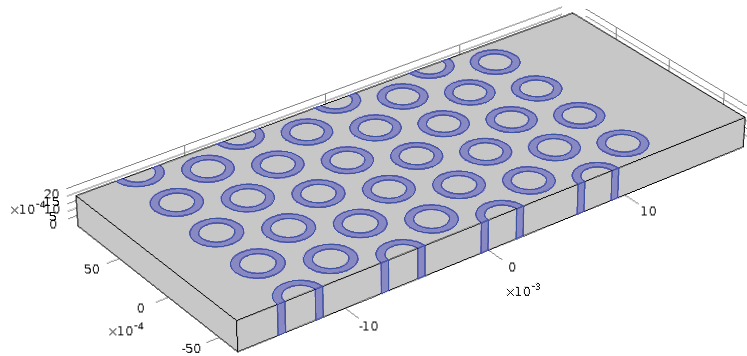


**Figure 9. Schematic of a cross-flow tritium removal facility**

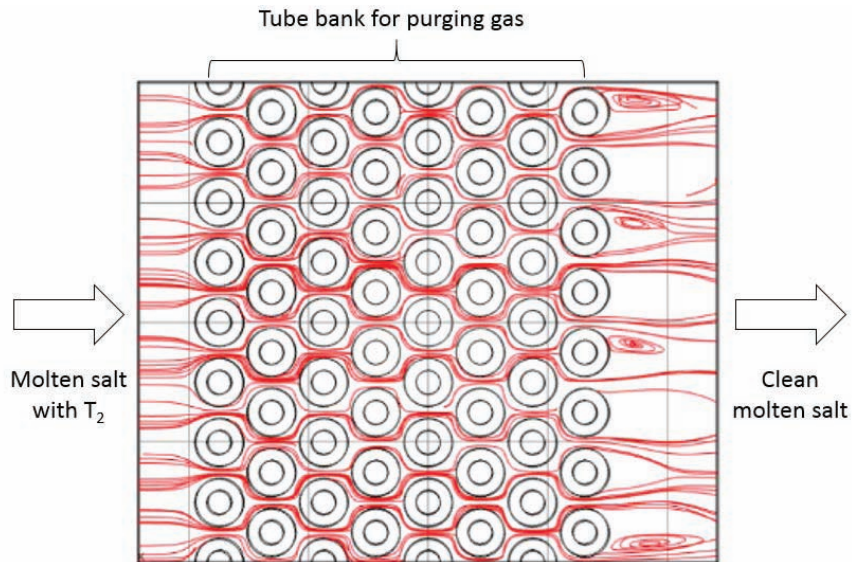


**Figure 10. Flow streamlines for the molten salt in the cross-flow design**

The results of two heat exchanger designs, namely the finned plate design and the wavy plate design suggest that it is reasonable to develop a design that can mix the molten salt flow. Thus the concept of a cross-flow tritium removal facility has been proposed. The geometry of the facility is shown in Figure 9 and is given in Table IV.

Figure 10 shows the molten salt flow stream lines in this design concept. The purging gas flows in the tubes. The tubes are staggered so that the stream containing the maximum H<sub>2</sub> concentration fully contacts with a tube and flows around the tube. In this way, not only the maximum concentration difference is assured at the mass transfer interface, but the flow is also well mixed.

For computer simulation, a unit model as shown in Figure 9 was built using COMSOL. The geometry dimensions and operation conditions are listed in Table IV. Stainless steel 316 was used as the structural material. For molten salt FLiBe is used and for purging gas, air is used. Hydrogen was used instead of Tritium. Since the model consists only of 8 rows of staggered tubes, the calculation was repeated 9 times, the inlet concentration of each calculation uses the outlet concentration of the previous one. The results are listed in Table V. From the results, the removal rate of H<sub>2</sub> stays constant as the total flowing length increases. Thus, for a 99% removal, the total length needed can be easily estimated as

$$L = 0.0277 \times \frac{1.8 \times 99\%}{0.00146} = 33.81 \text{ m} \quad (2)$$

**Table IV. Input of computer simulation of cross flow tritium removal facility**

Tube bank pitch [mm]	4	Molten salt flow rate [m/s]	0.1
Tube outer diameter [mm]	3	Purging gas flow rate [m/s]	40
Tube inner diameter [mm]	2	Tritium inlet concentration [mol/m <sup>3</sup> ]	1.8×10 <sup>-7</sup>
Tube wall thickness [mm]	0.5	Tritium removal percentage [%]	99

**Table V. Simulation results for the cross-flow tritium removal unit**

	Total FLiNaK flowing length [m]	H <sub>2</sub> concentration in FLiNaK [ $\times 10^{-7}$ mol/m <sup>3</sup> ]	Decrease [ $\times 10^{-7}$ mol/m <sup>3</sup> ]
<b>Initial</b>	0	1.8	
<b>1</b>	0.0277	1.79854	0.00146
<b>2</b>	0.0554	1.79708	0.00146
<b>3</b>	0.0831	1.79562	0.00146
<b>4</b>	0.1109	1.79416	0.00146
<b>5</b>	0.1386	1.7927	0.00146
<b>6</b>	0.1663	1.79124	0.00146
<b>7</b>	0.1940	1.78978	0.00146
<b>8</b>	0.2217	1.78832	0.00146
<b>9</b>	0.2494	1.78686	0.00146

## 2.6. Summary and Comparison of Tritium Removal Facility Design Concepts

Table VI summarizes the current design concepts for the tritium removal facility. For comparison, the mass flow rate of molten salt in each case has the uniform value of 1 m<sup>3</sup>/s. The total flow length of molten salt needed to achieve 99% removal is obtained from computer simulation. It is obvious that the cross-flow design achieves the smallest facility volume to fulfill 99% tritium removal. This design concept is also advantageous in aspects of manufacture and maintainance, since it adopts the setup of a cross-flow heat exchanger.

**Table VI. Comparison of tritium removal facility design concepts**

Design Concept	Mass Transfer Surface Area Per Unit Volume [m <sup>2</sup> /m <sup>3</sup> ]	Molten Salt Inlet Area [m <sup>2</sup> ]	Molten Salt Flow Rate [m/s]	Total Molten Salt Flow Length Needed [m] (99% removal of 1.8×10 <sup>-7</sup> mol/m <sup>3</sup> initial tritium concentration)	Advantages	Drawbacks
Helium Gas Purging Method (1 mm bubble diameter, ε=90%)	600	27.7	0.2	200	Post process does not require complicated methods.	To keep a high enough bubble volume fraction is not feasible.
Stainless Steel Packed Bed Scrubber (D20S40a)	354	0.79	6.975	2200	The packed bed facility design is mature.	Low efficiency of tritium removal. Facility too large.
Finned Plate Tritium Removal Facility Design	738	55.4	0.1	> 3000	The finned heat exchanger design is mature.	Low efficiency of tritium removal. Facility too large.
Wavy Plate Design	711	55.4	0.1	38	Relatively high tritium removal efficiency.	Dimensions of the facility are large.
Cross-Flow Tube Bank	1178	55.4	0.1	34	Relatively high tritium removal efficiency.	High molten salt pressure drop.

## 3. CONCLUSION

Based on the computer simulation of several design concepts for tritium removal facility used in FHRs, it is concluded that the key issues to consider are:

1. Large surface area to volume ratio;
2. Mixing of molten salt;
3. Large tritium concentration difference between molten salt side and absorbing/removing side.

Comparing current designs, the cross-flow design which resembles a heat exchanger is the most promising design concept. Further investigation may focus on the detailed geometry and operation conditions, thus optimizing the design.

## ACKNOWLEDGMENTS

This research is being performed using funding received from the U.S. Department of Energy (DOE) Office of Nuclear Energy's Nuclear Energy University Programs.

The computer simulation in this research is supported by Ohio Supercomputer Center (OSC).

## REFERENCES

1. M. Atlas, N. Brickner, W. Chen, D. Tsai, "Tritium Management Approach for FHRs Using Supercritical Steam, Open-Air Brayton, and Closed Gas Brayton Power Cycles," UCTBT-12-0006, Department of Nuclear Engineering, University of California, Berkeley, (2012).
2. R. E. Treybal, *Mass-transfer Operations*, McGraw-Hill, New York, USA (1980).
3. "COMSOL Packed bed reactor", <http://www.comsol.com/model/packed-bed-reactor-238>.
4. D.T. Ingersoll, C.W. Forsberg, L.J. Ott, D.F. Williams, J.P. Renier, D.F. Wilson, S.J. Ball, L. Reid, W.R. Corwin, G. D. Del Cul, P.F. Peterson, H. Zhao, P.S. Pickard, E.J. Parma, "Status of Pre-conceptual Design of the Advanced High-Temperature Reactor (AHTR)", Oak Ridge National Laboratory, (2004).
5. A. P. Fraas and M. N. Özişik, *Heat exchanger design*, Wiley, New York, USA (1965).